










**Effect of electron correlation on trielectronic-recombination rate coefficients for Be-like argon**Chun Yu Zhang <sup>1,2</sup> Si Jie Wu <sup>2</sup> Kai Wang <sup>3,4</sup> Ran Si <sup>2,\*</sup> Ke Yao <sup>2</sup> Zhong Kui Huang <sup>5</sup> Wei Qiang Wen <sup>5</sup>  
Xin Wen Ma <sup>5</sup> Chong Yang Chen <sup>2</sup> and N. R. Badnell<sup>1,†</sup><sup>1</sup>*Department of Physics, University of Strathclyde, Glasgow G4 0NG, United Kingdom*<sup>2</sup>*Shanghai EBIT Lab, Key Laboratory of Nuclear Physics and Ion-beam Application, Institute of Modern Physics, Department of Nuclear Science and Technology, Fudan University, Shanghai 200433, China*<sup>3</sup>*Department of Physics and Anhui Key Laboratory of Optoelectric Materials Science and Technology, Key Laboratory of Functional Molecular Solids, Ministry of Education, Anhui Normal University, Wuhu, Anhui 241000, China*<sup>4</sup>*Hebei Key Lab of Optic-electronic Information and Materials, The College of Physics Science and Technology, Hebei University, Baoding 071002, China*<sup>5</sup>*Institute of Modern Physics, Chinese Academy of Sciences, Lanzhou 730000, China*

(Received 17 June 2023; accepted 24 July 2023; published 2 August 2023)

The merged-beam rate coefficients of dielectronic and trielectronic recombinations (DR and TR) within  $\Delta N = 0$  channels for Be-like  $\text{Ar}^{14+}$  were measured by Huang *et al.* [*Astrophys. J. Supp. Ser.* **235**, 2 (2018)] at the cooler storage ring in Lanzhou, China. Meanwhile, theoretical data were also calculated with AUTOSTRUCTURE (AS) code for comparison with the measured resonance spectrum. However, the AS calculations significantly underestimated TR resonance strengths in most cases. In the present work, we find that the electron correlation between DR and TR resonance states with different captured electron principal quantum numbers ( $n$ ) for the captured electrons (multi- $n$  CI) can significantly increase the strength of TR resonances with  $n = 6$  and 7, which is confirmed through the relativistic distorted-wave (RDW) approximation in the flexible atomic code (FAC) and the semirelativistic distorted-wave (SRDW) approximation in the AS. The corresponding plasma rate coefficients show a significant increase and are in better agreement with the experiment, with differences from the experiment reduced to  $\sim 10\%$  in both photoionized plasmas (PP) and collisionally ionized plasmas (CP) temperature ranges, as opposed to the previous theoretical results that exhibited differences of up to  $\sim 30\%$  over the same temperature ranges. Taking into account the multi- $n$  CI could account for most of the discrepancy between existing theoretical calculations and experimental results. Understanding electron correlation and its consequences is important for obtaining accurate TR rate coefficients that will be useful for modelers assessing its role in describing non-local thermodynamic equilibrium astrophysical plasma.

DOI: [10.1103/PhysRevA.108.022801](https://doi.org/10.1103/PhysRevA.108.022801)**I. INTRODUCTION**

Dielectronic recombination (DR) is the dominant electron-ion recombination process in both photoionized plasmas (PP) and collisionally ionized plasmas (CP) [1–5]. DR establishes the ionization balance of elemental charge states in non-local thermodynamic equilibrium (non-LTE) plasmas. This is a basic building block for spectroscopic diagnostic modeling. Furthermore, DR satellite lines themselves can be used as temperature and density diagnostics for such plasmas [1].

In a single configuration approximation, the DR process involves only two interacting electrons. It includes two steps: a free electron is captured by the target ion while

simultaneously exciting a single bound electron, and then the resulting unstable doubly-excited state may radiatively stabilize. When electron correlation effects are taken into account, higher-order resonance recombination involving more than two electrons could occur. In the trielectronic recombination (TR) process, two core electrons are simultaneously excited during the attachment of a free electron, forming a triply excited intermediate state, which again may radiatively stabilize. The TR resonances were observed for the first time comparable in strength to their dielectronic counterparts in Be-like  $\text{Cl}^{13+}$  [4], where two  $2s$  electrons are simultaneously excited to a  $2p$  subshell. Subsequently, obvious TR contributions were also observed in other Be-like ions, such as  $\text{Ne}^{6+}$  [6,7],  $\text{Mg}^{8+}$  [8],  $\text{Si}^{10+}$  [7,9],  $\text{Ar}^{14+}$  [10],  $\text{Ca}^{16+}$  [11],  $\text{Ti}^{18+}$  [12], and  $\text{Fe}^{22+}$  [13].

The formation of the triply excited intermediate state involved in the TR process depends sensitively on configuration interaction (CI), which makes TR a challenge to atomic-structure calculations [4]. In general, both the state-of-the-art semirelativistic distorted-wave (SRDW) calculations [14] performed by using the AUTOSTRUCTURE (AS) package [15] and the relativistic distorted-wave (RDW) calculations [16]

\*rsi@fudan.edu.cn

†badnell@phys.strath.ac.uk

Published by the American Physical Society under the terms of the [Creative Commons Attribution 4.0 International license](https://creativecommons.org/licenses/by/4.0/). Further distribution of this work must maintain attribution to the author(s) and the published article's title, journal citation, and DOI.

performed using the flexible atomic code (FAC) [17] could reproduce the experimentally derived plasma rate coefficient in the PP and CP temperature ranges to within  $\sim 30\%$  or even better. However, significant differences could be seen between the calculated DR/TR rate coefficients and measured merged-beam recombination rate coefficients, especially for the TR resonances. For example, the original AS calculation for Be-like  $\text{Cl}^{13+}$  [4] increasingly underestimates the TR resonance strengths towards higher collision energies; the original AS calculation for Be-like  $\text{Ar}^{14+}$  [10] also significantly underestimates the TR resonance strengths, especially at  $\sim 11$  eV and  $\sim 23$  eV, and it could not reproduce well the resonances below 0.5 eV.

It is well known that an accurate description of low-energy DR/TR resonances is always a challenging task, due to the large uncertainty of calculated resonance energies and strong electron correlation effects between them. In a recent work [18], we studied the absolute DR rate coefficients of Na-like  $\text{Kr}^{25+}$  measured by employing the electron-ion merged-beam technique at the heavy-ion storage ring. Both the AS and FAC calculations could reproduce very well the experimental results if the electron correlation among the low-energy resonances of the (Ne-like core)  $3l8l'$  and  $4l4l''$  complexes, in particular the CI between  $3d8s$  and  $4s4d$ , was considered. The inclusion of CI among DR resonances with different principal quantum numbers  $n$  (multi- $n$  CI) for the captured electrons was also found to improve the agreement between the theoretical and experimental DR results of Ar-like  $\text{Fe}^{8+}$  in our recent work [19]. Such configuration mixing among the complexes with very different  $n$ -values of the captured electron was generally discarded in the previous FAC and AS DR calculations. Only CI among the target configurations plus the same captured electron principal quantum numbers  $n$  (single- $n$  CI) was included in previous FAC calculations. Only CI among the target configurations plus the same captured electron principal quantum numbers  $n$  and angular quantum numbers  $l$  (single- $nl$  CI) was considered in previous AS calculations. It should also be mentioned that in our FAC calculations, the positions for the low-energy DR resonances of Na-like  $\text{Kr}^{25+}$  were *ab initio* calculated using the relativistic many-body perturbation theory (RMBPT) [20,21], and were found to be in very good agreement with the measured ones [18].

A large-scale electron correlation is strongly required for TR resonances, due to the increase in the number and strength of radiative decay channels for the triply excited intermediate states. In this work, we continue to explore strategies to improve the calculated accuracy for low-energy TR resonances in Be-like  $\text{Ar}^{14+}$ . The low resonance energies arising from all possible  $1s^2 2l^2 n l'$  [ $n \leq 7, l' \leq (n-1)$ ] configurations are calculated with the RMBPT method. Using two different codes, FAC [22] and AS [23], we investigate the DR and TR rate coefficients for Be-like  $\text{Ar}^{14+}$  from the initial ground state ( $1s^2 2s^2 \ ^1S_0$ ). In addition, we analyze in detail how the multi- $n$  CI between DR and TR resonance states significantly increases the TR rate coefficients, which is cross-validated via FAC and AS calculations. The present total FAC and AS results including the enhanced TR resonances contributions agree better with the measured spectrum [10] than previous

calculations [10,14,16]. The present FAC and AS plasma rate coefficients agree with the experimentally deduced ones [10] within  $\sim 10\%$ , in both PP and CP temperature ranges. However, the previous theoretical calculations [10,14,16] are lower than the measurement by up to  $\sim 30\%$ .

The remainder of this paper is organized as follows. The theoretical methods and calculational procedure are outlined in Sec. II. In Sec. III, we present our FAC and AS results and compare them with measured values. The effect of multi- $n$  CI on TR resonance strengths is discussed in detail. A conclusion is given in Sec. IV.

## II. OUTLINE OF THEORY AND CALCULATION PROCEDURE

### A. Distorted-wave approach

In the independent process and isolated resonance approximations, DR resonance strength can be obtained by using the detailed balance principle

$$S_{ij} = \frac{g_j}{2g_i} \frac{\pi^2 \hbar^3}{m_e E_{ij}} A_{ji}^a B_j^r, \quad (1)$$

where  $i$  is the initial level of the recombining ion  $\text{Ar}^{14+}$  in the resonance capture process,  $j$  the resulting unstable doubly or triply excited intermediate level, and  $g_i$  and  $g_j$  are, respectively, statistical weights of  $i$  and  $j$  levels.

In the above,  $E_{ij} = E_j - E_i$  represents the resonance energy, and the DR resonance process occurs only when the kinetic energy of the incident electron equals  $E_{ij}$ . The autoionization rate  $A_{ji}^a$  from  $j$  to  $i$  can be expressed as

$$A_{ji}^a = 2 \sum_{\kappa} |\langle \Psi_i | \sum_{\substack{p,q \\ p < q}} \frac{2}{r_{pq}} | \Psi_j \rangle|^2, \quad (2)$$

where  $\Psi_j$  is the autoionizing state,  $\Psi_i$  the final state which has one less electron than  $\Psi_j$ ,  $\kappa$  the relativistic angular quantum number of the free electron, and  $r_{pq}$  the distance between two electrons  $p$  and  $q$  in the  $N+1$ -electron system.

Finally, the  $B_j^r$  indicates the DR radiative branching ratio, and it is defined as

$$B_j^r = \frac{\sum_f A_{jf}^r}{\sum_k A_{jk}^a + \sum_h A_{jh}^r}, \quad (3)$$

where  $k$  represents all possible autoionizing channels from  $j$ ,  $f$  the bound levels in the recombined ion  $\text{Ar}^{13+}$ , and  $h$  all possible radiative final states, including autoionizing levels  $j'$ . So,  $\sum_h A_{jh}^r = \sum_f A_{jf}^r + \sum_{j'} A_{jj'}^r$ . But, when the radiative decays to autoionizing levels, followed by radiative cascades (DAC) channels, are included, the  $B_j^r$  can be rewritten as

$$B_j^r = \frac{\sum_f A_{jf}^r + \sum_{j'} A_{jj'}^r B_{j'}^r}{\sum_k A_{jk}^a + \sum_h A_{jh}^r}. \quad (4)$$

Here,  $j'$  represents lower-lying ( $j' < j$ ) autoionizing levels which then radiatively cascade through levels of the recombined ion  $\text{Ar}^{13+}$ . The  $B_{j'}^r$  indicates the DR radiative branching ratio of state  $j'$  and it is defined the same as Eq. (4).

After summing all possible autoionization channels and averaging over the Maxwellian distribution of the electron

energy, the plasma rate coefficients for thermal equilibrium plasmas are given as [24]

$$\alpha(T_e) = \frac{h^3}{(2\pi m_e k_B T_e)^{3/2}} \sum_j \frac{g_j}{2g_i} A_{ji}^a B_j^r \exp\left(-\frac{E_{ij}}{k_B T_e}\right), \quad (5)$$

where  $h$  and  $k_B$  represent the Planck and Boltzmann constants, respectively.

### B. FAC and AS

We only give a brief description of FAC here, since more details have been discussed by Gu [25]. FAC [22], a fully relativistic program, is used to compute atomic structure and collision data. The results of atomic structure including energy levels, transition rates, and autoionization rates are obtained using the relativistic configuration interaction (RCI) method. The basic wave functions are derived from a local central potential that is self-consistently determined to represent electronic screening of the nuclear potential. The continuum processes are treated in an independent processes RDW approximation. Electron-electron and electron-photon interactions are treated with first-order perturbation theory in this code.

We also only outline the main points of AS code, and the in-depth details can be found in the work from Badnell *et al.* [15]. AS [23] is a general code for the description of a wide variety of bound-state, free-bound electron, and photon collision processes [26]. We use kappa-averaged relativistic wave functions and the full Breit interaction in the Pauli approximation. Similar to FAC, electron-electron and electron-photon interactions in AS calculations are treated with first-order perturbation theory. DR calculations are performed with a multiconfiguration Breit-Pauli (MCBP) implementation within an independent processes SRDW approximation.

It should be noted that the main differences between FAC and AS are that the former is fully relativistic and the radial orbitals for the construction of basis states are derived from a modified self-consistent Dirac-Fock-Slater iteration on a fictitious mean configuration with fractional occupation numbers, representing the average electron cloud of the configurations in calculations [25], while the latter is kappa-averaged relativistic and it uses the Thomas-Fermi-Dirac-Amaldi statistical gas potential [27]. Like FAC [25], it is a unique potential and it only depends on the nuclear charge and the number of electrons, if no radial scaling parameters are used [27].

### C. Calculation procedure

Using FAC, we have successfully performed the calculations of the resonance excitation rate coefficients for Ni-like Ta<sup>45+</sup> and Ni-like W<sup>46+</sup> [28–30], as well as the DR rate coefficients for Li-like Ca [31], C-like Ca [32], C-like Kr [33], Na-like Kr [18], Ni-like Au<sup>51+</sup> [34], Co-like ions [35–37], and Ar-like ions [19]. Using AS, a series of DR calculations for H-like through P-like isoelectronic sequences [5,14,38–51], Fe isonuclear sequence [52], and W isonuclear sequence [53–56] have been successfully performed by Badnell *et al.* Here also, by using FAC and AS, we carry out *ab initio*

calculations of the DR and TR rate coefficients for Be-like Ar<sup>14+</sup> from the initial ground state  $1s^2 2s^2 1S_0$ .

Our FAC and AS calculations are divided into two parts. The first is for  $\Delta N = 0$  ( $2 \rightarrow 2$ ) core-excitation channels that correspond to low-temperature DR or TR. The second is for  $\Delta N > 0$  ( $2 \rightarrow 3$ ,  $2 \rightarrow 4$ , and  $1 \rightarrow 2$ ) channels that correspond to high-temperature DR or TR. The autoionization channels and radiative decay channels involved in the present calculations can be presented as

$$1s^2 2s^2 + e^- \rightarrow \left\{ \begin{array}{l} 1s^2 2l^2 n' l'''' \\ 1s^2 2l 3l' n l'''' \\ 1s^2 2l 4l'' n l'''' \\ 1s 2l^3 n l'''' \end{array} \right\} \rightarrow \left\{ \begin{array}{l} 1s^2 2l n l'''' \\ 1s 2l^2 n l'''' \end{array} \right\} + e^- \\ \searrow \left\{ \begin{array}{l} 1s^2 2l^2 n' l'''' \\ 1s^2 2l 3l' n l'''' \\ 1s^2 2l 4l'' n l'''' \\ 1s 2l^3 n l'''' \end{array} \right\} + h\nu, \quad (6)$$

where  $l \leq 1$ ,  $l' \leq 2$ ,  $l'' \leq 3$ ;  $n' \leq 300$  for FAC but  $n' \leq 100$  for AS, and  $l'''' \leq 12$  for the  $\Delta N = 0$  core-excitation channels;  $n \leq 10$  and  $l'''' \leq 9$  for the  $\Delta N > 0$  core-excitation channels.

In order to analyze in detail the effect of the multi- $n$  CI between DR and TR resonance states, we perform two different calculations, which consider different CI scales, single- $n(l)$  CI and multi- $n$  CI. The multi- $n$  CI effect is cross-checked using FAC and AS codes. We consider the same CI scale as possible in FAC and AS calculations as the following:

(1) FAC single- $n$  CI: The CI among  $1s^2 2l n l''''$  ( $l \leq 1$ ,  $n \leq 10$ ,  $l'''' \leq 9$ ) but restricted within the same  $n$  is considered for the recombining ion Be-like Ar<sup>14+</sup>, and CI among  $1s^2 2l n' l'' n l'$  ( $n' \leq 4$ ,  $n \leq 10$ ) and  $1s 2l^3 n l''$  ( $n \leq 10$ ) but also restricted within the same  $n$  and  $n'$  is considered for the recombined ion B-like Ar<sup>13+</sup>.

(2) AS single- $nl$  CI: Similar to FAC single- $n$  CI, but the CI among the configurations mentioned above is additionally restricted within the same  $l''''$ .

(3) FAC and AS multi- $n$  CI: The CI among all possible  $1s^2 2l n l''''$  ( $l \leq 1$ ,  $n \leq 10$ ,  $l'''' \leq 9$ ) is considered for the recombining ion Be-like Ar<sup>14+</sup>, and CI among all possible  $1s^2 2l n' l'' n l'$  ( $n' \leq 4$ ,  $n \leq 10$ ) and  $1s 2l^3 n l''$  ( $n \leq 10$ ) is considered for the recombined ion B-like Ar<sup>13+</sup>.

In the present FAC calculations, the radial wave functions are optimized on the configurations  $1s^2 2l^3$  ( $l \leq 1$ ). The corresponding orbital occupation numbers are 2, 0.875, 0.875, and 1.25 for  $1s$ ,  $2s$ ,  $2p_{1/2}$ , and  $2p_{3/2}$  orbitals, respectively. Optimizing  $1s^2 2l^3$  ( $l \leq 1$ ) configurations give results a better agreement with the experimental results than  $1s^2 2l^2$  ( $l \leq 1$ ), the same as with Ref. [57]. Electric-dipole (E1) radiative rates and autoionization rates involving the  $n \leq 300$  ( $l \leq 12$ ) levels are explicitly calculated. The contributions of  $300 < n \leq 1000$  ( $l \leq 12$ ) resonances for plasma rate coefficients are included via the level-by-level extrapolation method, as discussed in Refs. [35,58].

All possible DAC channels with  $n \leq 13$  autoionizing levels are taken into account in our FAC calculations. The Breit interaction and the leading quantum electrodynamics (QED) corrections are fully considered in the present calculations.

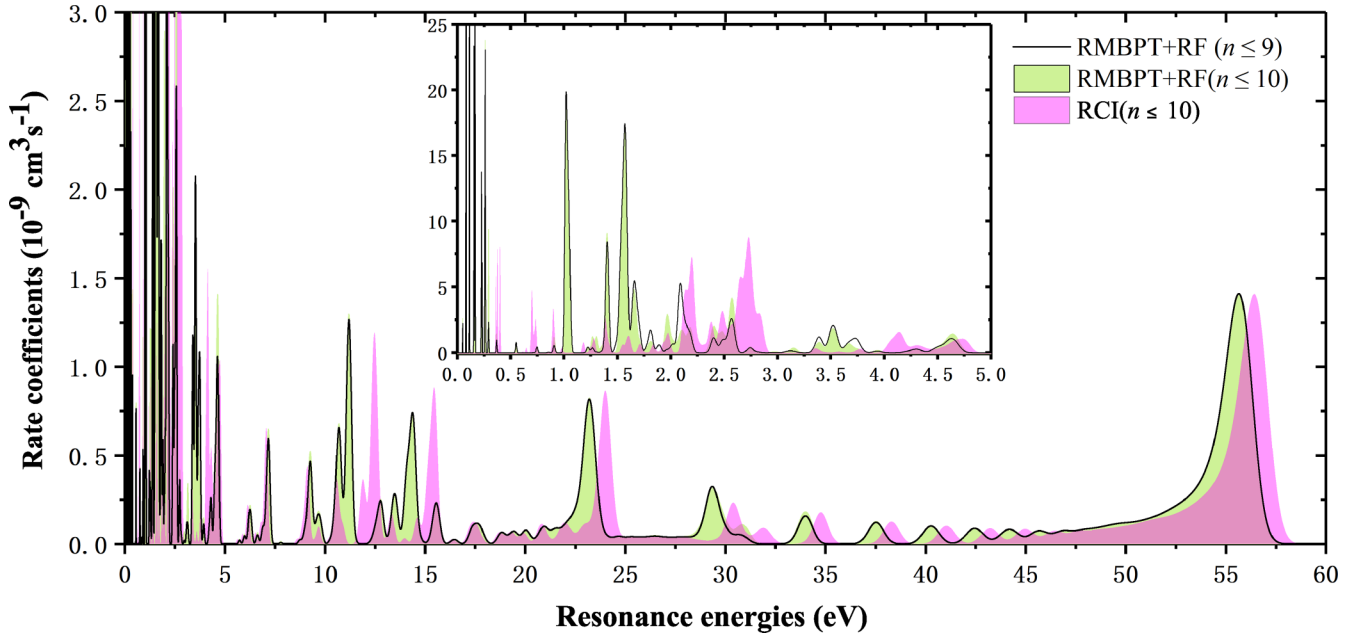


FIG. 1. Comparison of the present RMBPT + RF ( $n \leq 9$ ) (black solid curve), RMBPT + RF ( $n \leq 10$ ) (green shaded area), and RCI ( $n \leq 10$ ) (pink shaded area) total (DR + TR) rate coefficients. The RMBPT + RF ( $n \leq 9$ ) and RMBPT + RF ( $n \leq 10$ ) calculations respectively consider the multi- $n$  CI among  $n \leq 9$  and  $n \leq 10$  configurations, and their resonance energies are adjusted based on the RMBPT or RF results. The RCI ( $n \leq 10$ ) calculation also considers the multi- $n$  CI among  $n \leq 10$  configurations, but the resonance energies are from the RCI calculations. See the text for details.

In the multi- $n$  AS calculations, excitation energies, E1 radiative rates, and autoionization rates involving the  $n \leq 10$  ( $l \leq 9$ ) levels are calculated in the intermediate-coupling (IC) scheme with the MCBP approximation. The single- $nl$  radiative rates and autoionization rates for the high-lying  $11 \leq n \leq 100$  ( $l \leq 12$ ) resonances are calculated in the same fashion but with CI within the Be-like core only. The single- $nl$  rates for higher  $n$  up to 1000 are calculated using a quasi-logarithmically spaced set of  $n$  values, and interpolation is then used to obtain the remaining  $n$ .

All possible DAC channels with  $n \leq 10$  autoionizing levels are taken into account in our AS calculations. The Breit interaction and the leading QED corrections are also considered.

#### D. Adjustment and convergence monitor

It should be noted that the RCI and MCBP resonance energies should be used with caution for resonances below a few tens of electronvolts since the uncertainty of them is about a few electronvolts [16], thus adjustment according to more accurate calculations or measured values is necessary. We have successfully used the RMBPT [20,21] implemented in the FAC [22] to get the high-precision excitation energies of nonautoionization levels for a series of highly charged ions (HCIs) [59–72].

In this work, the RMBPT is used to study the excitation energies of autoionization levels for B-like  $\text{Ar}^{13+}$ . In our RMBPT calculations, all possible  $1s^2 2l^2 nl'$  ( $n \leq 7, l' \leq 6$ ) configurations are contained in the  $M$  space, and all possible configurations that are generated from single or double excitations of the  $M$  space are involved in the  $N$  space. The

maximum principal quantum numbers are, respectively, 150 and 70 for single and double excitations, and the maximum orbital quantum number is 20 in our RMBPT calculations.

The high- $n$  resonance energies can be estimated by a Rydberg formula (RF) which treats the Rydberg electron hydrogenically,

$$E_{nl} = E_{\text{exc}} - R \left( \frac{z}{n - \mu_l} \right)^2, \quad (7)$$

where  $E_{nl}$  is resonance energy for a given  $nl$  state,  $E_{\text{exc}}$  is core-excitation energy of the recombining ion,  $z$  is the charge state of the recombining ion,  $R$  represents the Rydberg energy, and  $\mu_l$  is named as the quantum defect that is obtained by the quantum defect theory (QDT).

The present  $n \geq 8$  resonance energies are shifted for an entire series according to the accurately measured core-excitation energies [73], which are compiled in the atomic spectra database (ASD) of the NIST [74]. However, the core-excitation energy of  $1s^2 2p^2 \ ^1D_2$  is not provided in NIST, then we get it from our recent calculation [67], which is 85.4889 eV. The ionization limitation of  $\text{Ar}^{13+}$ , referred to in Ref. [75], is  $-755.1639(46)$  eV.

To monitor the convergence of the present calculations of total (DR + TR) rate coefficients, we enlarge the electron correlation among all possible  $1s^2 2ln'l''nl'$  ( $n' \leq 4$ ) and  $1s2l^3nl'$  for  $\text{Ar}^{13+}$  by increasing  $n$  from 7 to 10 step by step. Figure 1 shows the present FAC multi- $n$  CI rate coefficients that are obtained by multiplying the resonance strengths with the electron-ion collision relative velocity and convolved with the Gauss distribution. The rate coefficients from  $n \leq 9$  calculations [labeled RMBPT + RF ( $n \leq 9$ )] and  $n \leq 10$

TABLE I. Comparison of the present RF, RCI, MCBP, and RMBPT resonance energies ( $E_{ij}$ , in eV), as well as FAC and AS multi- $n$  CI resonance strengths ( $S_{ij}$ , in  $10^{-18}$  cm<sup>2</sup> eV) with the peak fits of the experiment [10] below 0.5 eV resonance energies.

Experiment		This work						
$E_{ij}$	$S_{ij}$	Level	$E_{ij}$				$S_{ij}$	
			RF	RCI	MCBP	RMBPT	FAC	AS
0.08269(84)	10.57(15)	$2p^2(^3P)6d^4F_{3/2}$	0.1475	0.7189	0.5639	0.0782	5.70	7.87
		$2p^2(^3P)6p^4D_{5/2}$	0.1100	0.6109	0.5051	0.0934	0.18	0.07
		$2p^2(^3P)6s^4P_{5/2}$	0.1558	0.6443	0.5534	0.0936	0.87	2.37
						(6.75)	(10.3)	
0.14436(88)	13.32(15)	$2s2p(^1P)7p^2S_{1/2}$	0.3209	1.4132	1.3869	0.1251	3.40	5.50
		$2s2p(^1P)7p^2P_{3/2}$	0.2854	1.3754	1.2900	0.1255	4.40	9.38
		$2p^2(^3P)6p^4S_{3/2}$	0.1887	0.6980	0.6289	0.1577	7.58	4.52
						(15.4)	(19.4)	
0.23232(94)	17.78(17)	$2s2p(^1P)7p^2D_{3/2}$	0.3691	1.5478	1.6257	0.2006	2.37	4.52
		$2s2p(^1P)7p^2D_{5/2}$	0.3431	0.8993	0.7863	0.2100	5.36	7.15
		$2s2p(^1P)7p^2P_{1/2}$	0.4843	1.5884	1.6363	0.2720	2.27	2.61
						(10.0)	(14.3)	
0.3173(14)	8.25(17)	$2p^2(^3P)6d^4F_{5/2}$	0.3240	1.3859	1.3365	0.3030	4.36	5.73
		$2p^2(^3P)6p^4P_{1/2}$	0.4414	0.7350	0.8811	0.3354	1.93	0.01
		$2p^2(^3P)6p^2D_{3/2}$	0.4487	0.9787	0.9481	0.4126	0.33	0.03
						(6.62)	(5.77)	

calculations [labeled RMBPT + RF ( $n \leq 10$ )] are compared in Fig. 1. Their resonance energies for  $n \leq 7$  levels are adjusted based on the RMBPT results, and NIST core-excitation energies are used to adjust the  $8 \leq n \leq 300$  levels via the RF. Most of the differences between RMBPT + RF ( $n \leq 9$ ) and RMBPT + RF ( $n \leq 10$ ) results are within 1%. Good convergence is achieved when  $n$  is up to 10.

### III. RESULTS AND DISCUSSION

#### A. Resonance energies

The RCI ( $n \leq 10$ ) and RMBPT + RF ( $n \leq 10$ ) results are also compared in Fig. 1. The former indicates the resonance energies from RCI calculations, and the latter represents that the RCI resonance energies are corrected by the RMBPT results or the NIST core-excitation energies. The two calculations consider the same CI scale, multi- $n$  CI ( $n \leq 10$ ), which can be seen in Sec. II C. It can be obviously seen that the RCI resonance energies are generally higher than the adjusted results, RMBPT + RF, about 1–2 eV in most cases. As we can see from the inserted figure in Fig. 1, the spectra features between RCI and RMBPT + RF results are significantly different when the resonance energy is lower than 5 eV. Therefore, the adjustment for RCI resonance energies according to the RMBPT results or NIST core-excitation energies via the RF is necessary.

As is well known, the RF is convenient and quick to estimate the resonance energies of higher- $n$  levels when the outermost-shell electron can be treated as a spectator electron. However, it should be used with caution for the lower- $n$  values. In Table I we compare the resonance energies from the present RF, RCI, MCBP, and RMBPT calculations with the peak fits of the experimental [10] ones for resonances below 0.5 eV. There are three calculated levels that are associated

with each peak fitted in the experiment. The experimental value is listed on the same line as the one of the three with the largest calculated resonance strength.

From Table I, we can see that the RCI and MCBP resonance energies are higher than the experimental peak fits by up to  $\sim 1$  eV. It can also be found that the present RMBPT resonance energies are in good agreement with the experimental values within 0.02 eV. The RF resonance energies are in much better agreement with RMBPT than RCI and MCBP, but they depart from the experimental peak fits for the levels  $2p^2(^3P)6d^4F_{3/2}$  and  $2s2p(^1P)7p^2D_{5/2}$  by up to 0.06 eV and 0.1 eV, respectively, which can sensitively result in a dramatic uncertainty of DR and TR rate coefficients. Thus, the RF is not suitable for accurately predicting the resonance energies of lower- $n$  levels, such as the  $n = 6$  and 7 levels.

Additionally, the comparison of all of the  $2l^2nl'$  ( $n \leq 7, l' \leq 6$ ) resonance energies from the present RCI, MCBP, RF, and RMBPT calculations can be seen in the Supplemental Material [76]. The average difference  $\pm$  standard deviation of the present RCI, MCBP, and RF resonance energies from RMBPT results are found to be  $0.87 \text{ eV} \pm 0.40 \text{ eV}$ ,  $0.78 \text{ eV} \pm 0.39 \text{ eV}$ , and  $0.03 \text{ eV} \pm 0.04 \text{ eV}$ , respectively.

#### B. DR and TR rate coefficients

In Table I, as noted above, there are three calculated levels corresponding to each peak fitted in the experiment, and they are listed at each block. The sum of these three resonance strengths corresponding to each peak fitted in the experiment is listed in brackets at the bottom of each block, which is the final result from the present calculations corresponding to each observed resonance strength. As shown in Table I, the present FAC and AS multi- $n$  total resonance strengths  $S_{ij}$  deviate from the measurement by  $\sim 40\%$ . This may be

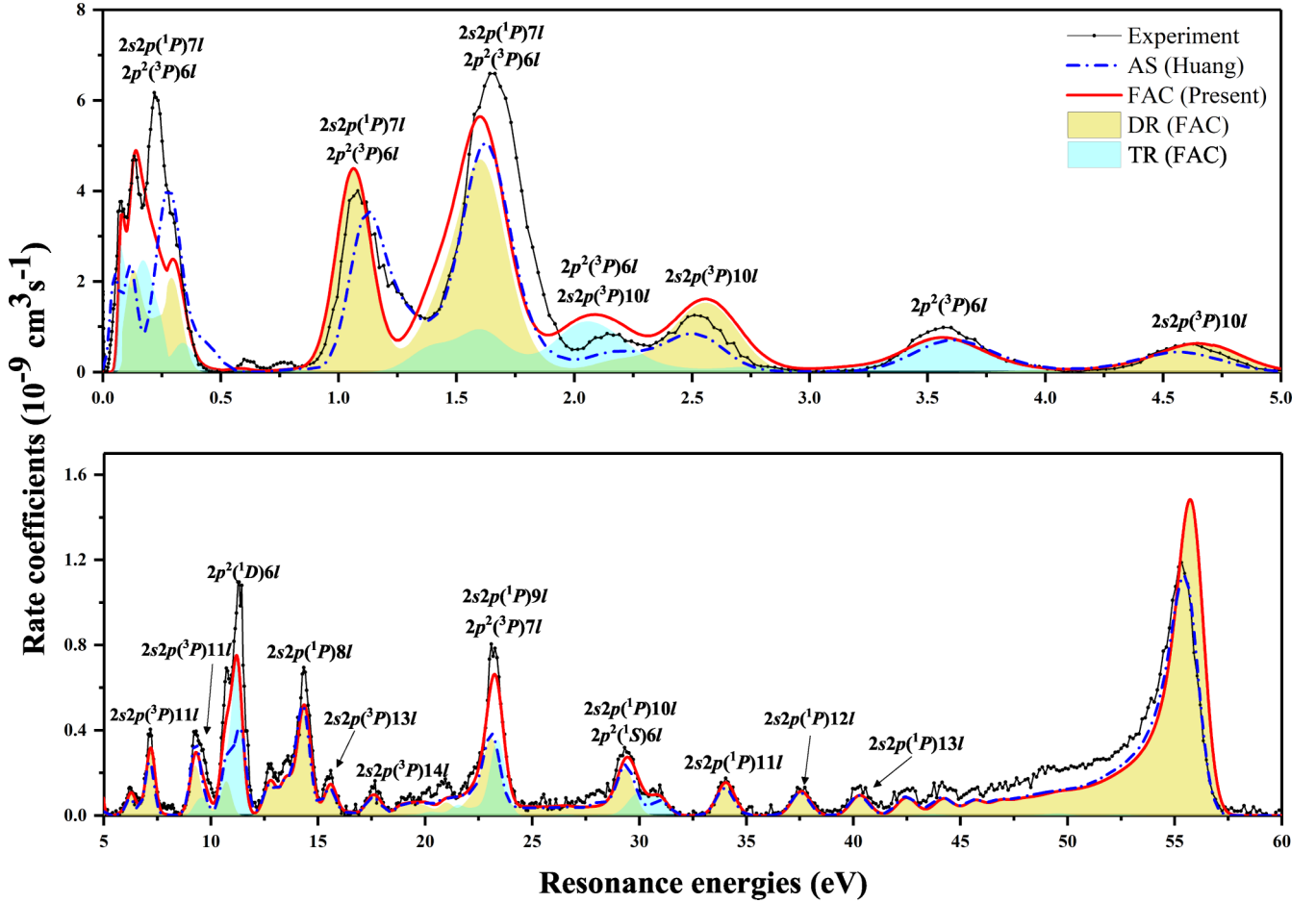


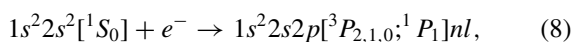
FIG. 2. Comparison of the present FAC total (DR + TR) rate coefficients (red solid curve) with the previous AS calculations [10] (blue dash-dot curve) and measured recombination spectrum [10] (black data points). The present DR and TR parts are shown by the yellow-shaded areas and the cyan-shaded areas, respectively. The strong DR (TR) resonance peaks are labeled by the doubly (triply) excited intermediate states based on the present FAC calculations.

because the resonance strengths near the ionization threshold are extremely sensitive to the resonance positions, even though our RMBPT results have already greatly improved them. Determining the resonance positions accurately enough near the ionization threshold is still a challenge.

In Fig. 2, the present FAC multi- $n$  CI rate coefficients are compared with the previous AS calculations and the measured spectrum [10]. The present rate coefficients are obtained by convoluting the product of resonance strengths and electron collision relative velocity with the experimental energy distribution [10]. A flattened Maxwellian electron energy distribution is used as described in Ref. [5], where the parallel and perpendicular temperatures are 2.40 meV and 11.91 meV, respectively.

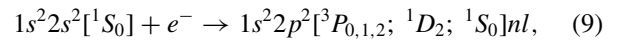
The strong resonance peaks are labeled based on the present FAC calculation, and the core electrons  $1s^2$  are omitted. The DR and TR parts shown in Fig. 2 are separated according to doubly and triply excited states, respectively.

The DR resonance process for  $\text{Ar}^{14+}$  recombining to  $\text{Ar}^{13+}$  can be represented by



which is associated with the doubly excited states  $2s 2p ({}^3P_{0,1,2}) nl$  and  $2s 2p ({}^1P_1) nl$  and gives rise to two sets of strong peaks at lower energies. The regular Rydberg series of  $2s 2p ({}^1P_1) nl$  dominates at higher energies and converges to the limit at 56.063 eV [74], giving rise to the characteristic Rydberg peak.

The TR resonance process for  $\text{Ar}^{14+}$  recombining to  $\text{Ar}^{13+}$  can be represented by



which is associated with the triply excited states  $2p^2 ({}^3P_{0,1,2}; ^1D_2; ^1S_0) nl$ . The corresponding TR rate coefficients are comparable with their DR counterparts at resonance energies lower than 32 eV in the spectrum.

We note that this definition of DR and TR is based upon the configuration labels associated with each resonance. But configuration is not a good quantum number. Indeed, as we observe, autoionizing configurations are highly mixed. Thus, two different calculations, even with the same code, which use different atomic structures (distorted-wave potential, Hamiltonian operators, etc.) can label a resonance as DR in one calculation and TR in another, and vice versa. At the

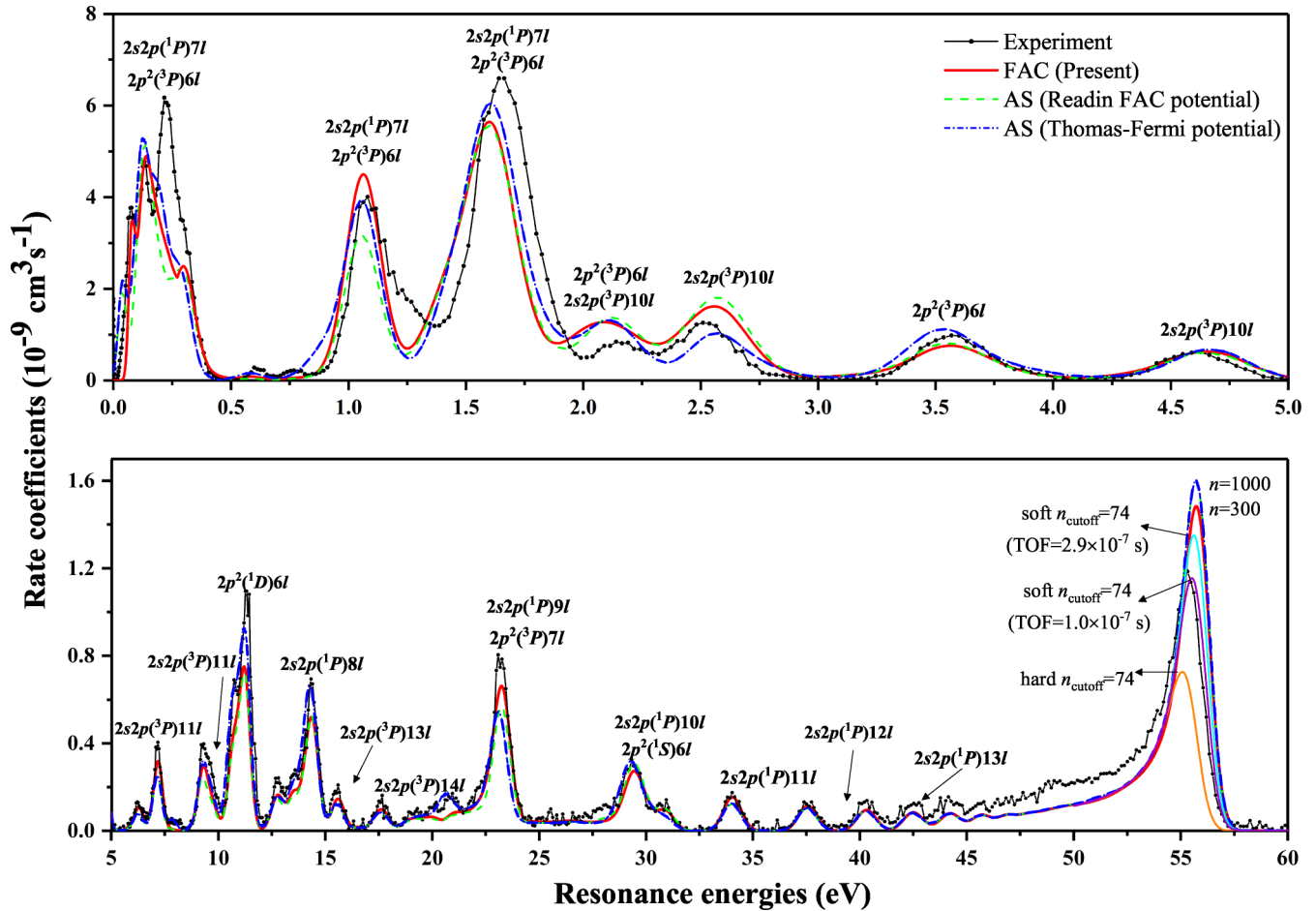


FIG. 3. Comparison of the present FAC rate coefficients (red solid curve) with the AS calculations where the FAC potential is directly read in AS procedure (green dash curve) and based on the Thomas-Fermi potential (blue dash-dot curve). The measured recombination spectrum [10] (black data points) is also presented. For the characteristic Rydberg peak, the hard cutoff  $n_{\text{cutoff}} = 74$  (orange solid curve), soft cutoff  $n_{\text{cutoff}} = 74$  (TOF =  $1 \times 10^{-7}$  s, purple solid curve), and soft cutoff  $n_{\text{cutoff}} = 74$  (TOF =  $2.9 \times 10^{-7}$  s, cyan solid curve) results are shown as well.

end of the day, the only meaningful quantity is the sum of the two.

In the previous AS calculations [10], only the  $2s^2$ ,  $2s2p$ , and  $2p^2$  configurations were considered for Be-like  $\text{Ar}^{14+}$  and  $2s^22p$ ,  $2s2p^2$ , and  $2p^3$  configurations for B-like  $\text{Ar}^{13+}$ , and only the single- $n(l)$  CI the same as that discussed in Sec. II C was considered. It can be found from Fig. 2 that some TR resonance strengths from the previous AS calculations [10] are significantly weaker than the measurement, such as those at  $\sim 1.62$  eV,  $\sim 11.2$  eV, and  $\sim 23.4$  eV positions. In the present calculations, not only single- $n(l)$  CI but also multi- $n$  CI are considered. From Fig. 2, we can see that the present FAC rate coefficients are in better agreement with the experimental values [10] than previous AS results [10] at  $\sim 1.62$  eV,  $\sim 11.2$  eV, and  $\sim 23.4$  eV positions. These significant enhancements are attributed to the multi- $n$  CI effect, see the detailed discussion in Sec. III C.

As mentioned in Sec. II B, the radial potentials generated from FAC [23] and AS [22] are different. To remove the difference caused by the radial potential, we perform an AS calculation where the potential obtained from FAC is directly read in the AS procedure, which is labeled as AS (Readin FAC

potential) in Fig. 3. One can see that the AS (Readin FAC potential) result is in excellent agreement with the FAC result except for the rate coefficients at  $\sim 1.1$  eV, where the autoionization rates are quite sensitive since the  $2s2p7d$  and  $2p^26p$  configurations are strongly mixed. Using the Thomas-Fermi potential, we get another AS result labeled AS (Thomas-Fermi potential) in Fig. 3. The differences between our FAC and AS (Thomas-Fermi potential) results shown in Fig. 3 are mainly from the different potentials used in FAC and AS rather than relativistic effects. Like our FAC results, it also shows that the multi- $n$  CI significantly enhances the present AS rate coefficients at  $\sim 1.62$  eV,  $\sim 11.2$  eV, and  $\sim 23.4$  eV positions.

For the characteristic Rydberg peak at the limit position 56.063 eV [74] in Fig. 3, the calculated FAC (to  $n = 300$ ) and AS (to  $n = 1000$ ) rate coefficients are much larger than the experiment. This is due to the field ionization of weakly bound high- $n$  Rydberg states which occurs primarily due to the charge-separating dipole magnet. The estimated (hard) cutoff quantum number is  $n_{\text{cutoff}} = 74$  in the experiment [10]. It is clear from Fig. 3 that the use of this hard cutoff underestimates the experiment significantly here.

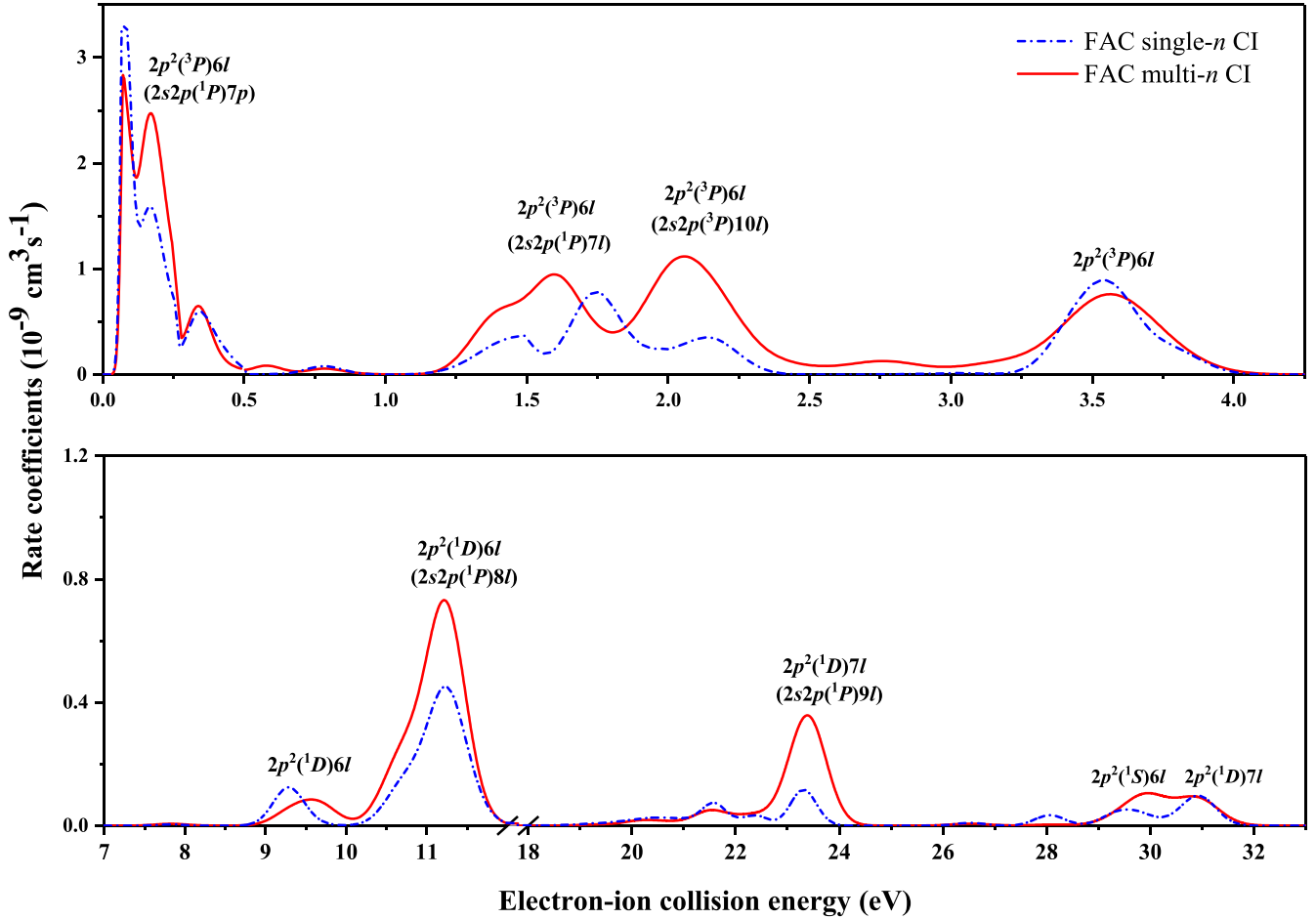


FIG. 4. Comparison of TR rate coefficients from the present FAC single- $n$  CI (blue dash-dot line) and multi- $n$  CI (red solid line) calculations. The strong TR resonance peaks are labeled by the triply excited intermediate states based on the present FAC calculations, and the ones in brackets are the doubly excited intermediate states that mix strongly with the corresponding triply ones.

We can model the characteristic Rydberg peak of the experiment [10] much better by considering the time-of-flight (TOF) of the recombined ions from the cooler to analyzer magnet. This allows states with  $n > 74$  to radiatively decay to  $n' < 74$  before reaching the magnet—this is known as a soft cutoff [5,77]. From Fig. 3, it can be seen that a TOF of  $1 \times 10^{-7}$  s fits the experiment best. But, using the expected experimental TOF of  $2.9 \times 10^{-7}$  s leads to a result that is somewhat larger. Nevertheless, the soft cutoff is much improved over the hard cutoff result but clearly still does not fully model the survival of the recombined ions to the detector.

### C. The effect of multi- $n$ CI

We compare the TR rate coefficients from the present single- $n$  CI and multi- $n$  CI calculations in Fig. 4 so as to demonstrate the importance of the multi- $n$  CI for TR rate coefficients.

As we noted above, the rate coefficients labeled TR are artificially distinguished from DR ones according to their configuration labels, which are not good quantum numbers. This labeling changes for some sensitive resonance states which mixed strongly in different calculations, such as the present

FAC and AS calculations. Therefore, only the present FAC results are shown in Fig. 4. It can be clearly found that the multi- $n$  CI significantly enhances the TR rate coefficients at  $\sim 1.62$  eV,  $\sim 11.2$  eV, and  $\sim 23.4$  eV positions.

We present the level energies of DR and TR resonance states with different principal quantum numbers  $n$  for captured electrons in Fig. 5. It can be seen that the resonance energies of the TR states  $2p^26l$  lie close to those of the DR states  $2s2p7l$  at 0.2 eV and 1.62 eV; to  $2s2p8l$  at 10.8 eV and 11.2 eV; and to  $2s2p10l$  at 2.1 eV and 29.5 eV. The resonance energies of the TR states  $2p^27l$  lie close to those of the DR states  $2s2p9l$  at 23.4 eV. Strong level mixing occurs at these resonance positions as evidenced by our multi- $n$  DR + TR results.

In Table II, we take the TR resonance strengths around 11.2 eV as an example to compare the FAC single- $n$  CI and multi- $n$  CI calculations. The autoionization rates  $A_{jk}^a$  from  $j$  to  $k$ , the total radiative decay rates  $\sum_h A_{jh}^r$  from  $j$  to all possible lower levels  $h$ , and the radiative branching ratios  $B_j^r$  are listed as well. It is only possible for  $j$  around 11.2 eV to autoionize to the ground level  $1s^22s^2\ ^1S_0$  since the core-excitation energy of the first excited level  $2s2p\ ^3P_0$  in  $\text{Ar}^{14+}$  is 28.353(4) eV [74]. In this case,  $A_{jk}^a$  is equivalent to  $A_{ji}^a$ , i.e., both  $k$  and  $i$



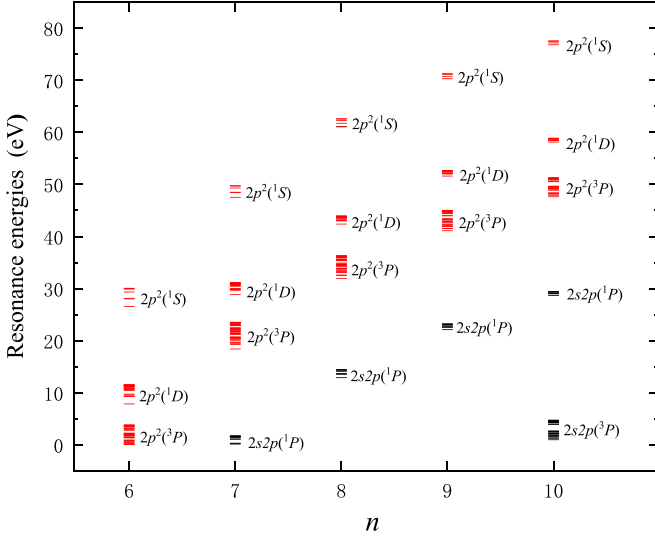


FIG. 5. Resonance energies of DR resonance states (black line) and TR resonance states (red line) as a function of complex  $n$  are presented. They are labeled by the core-excited configurations.

are the ground state  $1s^2 2s^2 \ ^1S_0$ . In our single- $n$  CI calculation, the great majority of  $A_{jk}^a$  around 11.2 eV are far less than the corresponding  $\sum_f A_{jf}^r$ . When further adding the multi- $n$  CI into our multi- $n$  CI calculation, most of the  $A_{jk}^a$  are increased by about an order of magnitude or more, while the  $\sum_f A_{jf}^r$  are hardly affected by the additional multi- $n$  CI—the changes are within 5%. This leads to a significant net increase in the TR resonance strengths in the multi- $n$  CI case over those in the single- $n$  CI case.

We take the TR resonance state  $2p^2(^1D)6f \ ^2H_{11/2}$  listed in Table II as an example, the  $A_{jk}^a$  from  $2p^2(^1D)6f \ ^2H_{11/2}$  to  $2s^2 \ ^1S_0$  increased by a factor of 19.5 (from  $2.56 \times 10^{10} \text{ s}^{-1}$  to  $4.99 \times 10^{11} \text{ s}^{-1}$ ), due to the multi- $n$  CI. And the corresponding  $B_j^r$  of  $2p^2(^1D)6f \ ^2H_{11/2}$  state in multi- $n$  CI calculations is declined by a factor of 3.48 compared to that calculated in single- $n$  CI mode (from 0.87 to 0.25). Combining  $A_{jk}^a$  and  $B_j^r$  of the  $2p^2(^1D)6f \ ^2H_{11/2}$  state in multi- $n$  CI calculations, based on Eq. (1), the resonance strength  $S_{ij}$  of this state is enhanced by a factor of 5.55 compared to the single- $n$  CI results (from  $5.93 \times 10^{-20} \text{ cm}^2 \text{ eV}$  to  $3.29 \times 10^{-19} \text{ cm}^2 \text{ eV}$ ).

TABLE II. Comparison of the resonance strengths ( $S_{ij}$ , in  $10^{-20} \text{ cm}^2 \text{ eV}$ ) of the TR resonance states  $j$  around 11.2 eV from the present FAC single- $n$  CI and multi- $n$  CI calculations. The resonance energies ( $E_{ij}$ , in eV), the autoionization rates  $A_{jk}^a$  (in  $10^{10} \text{ s}^{-1}$ ) from  $j$  to  $k$ , the total radiative decay rates  $\sum_h A_{jh}^r$  (in  $10^{10} \text{ s}^{-1}$ ) from  $j$  to  $h$  ( $h$  represents all possible lower levels of the transitions from  $j$ ), and the corresponding radiative branching ratios  $B_j^r$  are listed as well.

$E_{ij}$	$j$ level	Single- $n$ CI				Multi- $n$ CI			
		$A_{jk}^a$	$\sum_h A_{jh}^r$	$B_j^r$	$S_{ij}$	$A_{jk}^a$	$\sum_h A_{jh}^r$	$B_j^r$	$S_{ij}$
11.201	$2p^2(^1D)6f \ ^2H_{9/2}$	2.60	17.7	0.87	5.01	49.6	16.5	0.25	27.3
11.210	$2p^2(^1D)6f \ ^2H_{11/2}$	2.56	17.7	0.87	5.93	49.9	16.5	0.25	32.9
11.274	$2p^2(^1D)6h \ ^2I_{13/2}$	3.17	6.63	0.68	6.59	23.6	6.32	0.21	15.3
11.277	$2p^2(^1D)6h \ ^2K_{15/2}$	3.17	6.62	0.68	7.52	23.6	6.32	0.21	17.5
11.302	$2p^2(^1D)6g \ ^2I_{11/2}$	5.25	9.87	0.65	9.00	54.6	9.33	0.15	20.9
11.308	$2p^2(^1D)6g \ ^2I_{13/2}$	5.25	9.87	0.65	10.5	54.7	9.33	0.15	24.4

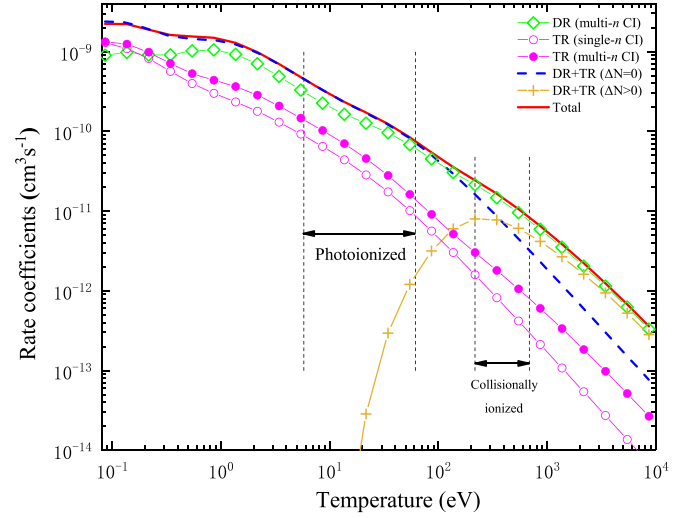


FIG. 6. The DR (green diamond), TR (pink solid circle), and total (red solid line) plasma rate coefficients from the present FAC multi- $n$  CI calculations are presented. The TR ones calculated in FAC single- $n$  CI case are shown by the pink hollow circle for comparison. The contributions from  $\Delta N = 0$  channels (blue dash line) and  $\Delta N > 0$  channels (yellow plus) are presented as well.

The same case also occurs in the TR resonance states  $j$  around 23.4 eV as shown in Table III. When additionally considering the multi- $n$  CI, most of  $A_{jk}^a$  increase significantly, while  $\sum_f A_{jf}^r$  are almost unchanged. For instance, additionally including multi- $n$  CI causes an increase in the  $A_{jk}^a$  from  $2p^2(^3P)7f \ ^4G_{11/2}$  to  $2s^2 \ ^1S_0$  by a factor of 550 (from  $3.00 \times 10^8 \text{ s}^{-1}$  to  $1.65 \times 10^{11} \text{ s}^{-1}$ ). And the  $B_j^r$  of the  $2p^2(^3P)7f \ ^4G_{11/2}$  state in multi- $n$  CI calculations is declined by a factor of 2.50 (from 1.00 to 0.40), compared to that calculated in single- $n$  CI mode. Combining  $A_{jk}^a$  and  $B_j^r$  of the  $2p^2(^3P)7f \ ^4G_{11/2}$  state, the resonance strength  $S_{ij}$  of this state is enhanced by a factor of 211 (from  $4.00 \times 10^{-22} \text{ cm}^2 \text{ eV}$  to  $8.42 \times 10^{-20} \text{ cm}^2 \text{ eV}$ ) due to the multi- $n$  CI effect.

#### D. Plasma rate coefficients

The DR, TR, and total (DR + TR) plasma rate coefficients for  $\text{Ar}^{14+}$  from the present FAC multi- $n$  CI calculations are presented in Fig. 6. The TR ones from FAC single- $n$  CI

TABLE III. Same as Table II but for the TR resonance states  $j$  around 23.4 eV.

$E_{ij}$	$j$ level	Single- $n$ CI				Multi- $n$ CI			
		$A_{jk}^a$	$\sum_h A_{jh}^r$	$B_j^r$	$S_{ij}$	$A_{jk}^a$	$\sum_h A_{jh}^r$	$B_j^r$	$S_{ij}$
23.335	$2p^2(^3P)7f^4G_{11/2}$	0.03	12.1	1.00	0.04	16.5	11.4	0.40	8.42
23.364	$2p^2(^3P)7f^2G_{9/2}$	0.02	11.9	1.00	0.03	16.7	11.1	0.40	7.01
23.416	$2p^2(^3P)7f^4F_{7/2}$	0.72	12.0	0.94	0.57	11.6	11.7	0.50	4.91
23.433	$2p^2(^3P)7f^4F_{9/2}$	0.01	11.6	1.00	0.01	5.31	11.1	0.67	3.78
23.461	$2p^2(^3P)7f^4F_{5/2}$	0.05	11.4	0.95	0.03	32.9	12.2	0.26	5.46
23.476	$2p^2(^3P)7h^4I_{15/2}$	0.07	4.86	0.98	0.12	19.3	4.67	0.18	5.79
23.485	$2p^2(^3P)7i^2K_{15/2}$	0.02	3.71	0.98	0.04	5.39	3.59	0.37	3.34
23.487	$2p^2(^3P)7i^4K_{17/2}$	0.02	3.71	0.98	0.04	5.45	3.58	0.37	3.78

calculations are also shown in Fig. 6 for comparison. The vertical dash bars denote the boundaries of the PP and CP temperature ranges, defined to be where the fractional abundance of this ion is 10% of its maximum [78,79]. The TR contribution to the total plasma rate coefficients in the PP and CP temperature ranges is  $\sim 30\%$  and  $\sim 10\%$ , respectively. It is found that TR plasma rate coefficients from single- $n$  CI calculations are increased by about 60% by the multi- $n$  CI effect in the PP and CP temperature ranges.

Moreover, the contributions from  $\Delta N = 0$  and  $\Delta N > 0$  core-excitation channels, based on our FAC multi- $n$  CI results, are also separately shown in Fig. 6. As we can see,  $\Delta N = 0$  core-excitation channels dominate in the PP temperature range. As the temperature increases, the DR and TR plasma rate coefficients associated with  $2s \rightarrow 3l$  core-excitation channels start to contribute and account for about 30% – 50% of the total plasma rate coefficients in the CP temperature range. As the temperature increases further, the  $2s \rightarrow 4l$  and  $1s \rightarrow 2l$  core-excitation channels start to

contribute as well, and they account for  $\sim 30\%$  of the total plasma rate coefficients by 10000 eV. In total, the contribution from these  $\Delta N > 0$  core-excitations is  $\sim 70\%$  of the total plasma rate coefficients by 10000 eV.

It should be mentioned also that the contribution of DAC channels to the total plasma rate coefficients is found to be less than 2%.

Furthermore, we compare the present FAC  $\Delta N = 0$  plasma rate coefficients with results derived from the measurement [10] in Fig. 7. Also shown are the present ( $\Delta N = 0 + \Delta N > 0$ ) FAC and AS results, the AS results from Colgan *et al.* [14], and the FAC results from Gu [16]. We find that the present FAC and AS results are in good agreement with the measurement, to within  $\sim 10\%$  in both the PP and CP temperature ranges. However, the previous theoretical results [10,14,16] are smaller than the experiment, by up to  $\sim 30\%$  over the same temperature ranges. The improved agreement of the present results is mainly attributed to the multi- $n$  CI effect. This kind of electron correlation was neglected by these previous calculations.

In order to make it convenient to use the present FAC and AS multi- $n$  CI results in plasma modeling, the present plasma rate coefficients are fitted by

$$\alpha(T_e) = \sum_i c_i \left( \frac{E_i}{T_e} \right)^{3/2} \exp\left( -\frac{E_i}{T_e} \right). \quad (10)$$

The fit parameters of  $c_i$  and  $E_i$  are listed in Table IV for  $\Delta N = 0$  channels and  $\Delta N > 0$  channels, and they can reproduce the present results within 2%.

#### IV. CONCLUSION

The present DR and TR rate coefficients of  $\text{Ar}^{14+}$  forming  $\text{Ar}^{13+}$  are calculated with the RDW approximation implemented in the FAC and the SRDW approximation implemented in the AS. We adopted two strategies to handle the existing challenges to theory, viz. the need to improve the accuracy of the position of low-energy resonances (DR + TR) and the size of TR resonance strengths themselves. Firstly, the low-energy resonance positions for the  $n \leq 7$  levels have been calculated using the RMBPT method. Secondly, by additionally considering multi- $n$  CI, the present TR resonance strengths are significantly increased, which is cross-validated by the results from our FAC and AS calculations. The TR plasma rate coefficients from single- $n$  CI calculations are

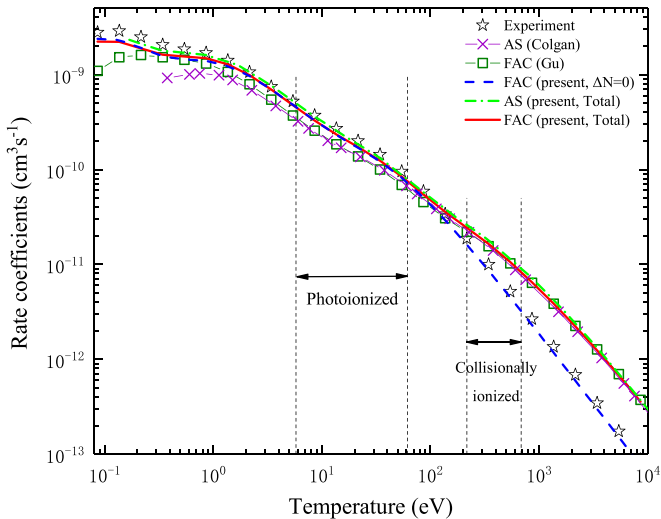


FIG. 7. Comparison of different theoretical calculations with the derived plasma rate coefficients from the measurement [10]. The present  $\Delta N = 0$  FAC, total ( $\Delta N = 0 + \Delta N > 0$ ) FAC, and total AS results are plotted by the blue dash line, red solid line, and green dash-dot line, respectively. The FAC results from Gu [16] are shown by the green square. The AS results from Colgan *et al.* [14] were updated on the website of Atomic and Molecular Diagnostic Processes in Plasmas [80], which are shown by the purple cross.

TABLE IV. The fitted coefficients  $c_i$  (in  $10^{-10} \text{ cm}^3 \text{ s}^{-1}$ ) and  $E_i$  (in eV) for the present FAC and AS multi- $n$  CI plasma rate coefficients of  $\Delta N = 0$  channels and  $\Delta N > 0$  channels in Be-like  $\text{Ar}^{14+}$ . Numbers in the squared brackets are powers of 10.

No.	$\Delta N = 0$		$\Delta N > 0$	
	$c_i$	$E_i$	$c_i$	$E_i$
FAC:				
1	3.253[1]	1.436[-1]	3.647[-2]	1.723[2]
2	2.616[1]	1.500[-1]	4.602[-2]	2.933[2]
3	8.464[0]	6.201[-1]	4.817[-2]	4.580[2]
4	2.004[1]	1.704[0]	8.470[-2]	4.580[2]
5	3.487[0]	4.351[0]	2.660[-3]	1.688[3]
6	1.840[0]	1.471[1]	5.070[-3]	2.889[3]
7	1.218[0]	4.844[1]	4.459[3]	6.869[9]
AS:				
1	3.398[1]	1.531[-1]	3.559[-2]	1.714[2]
2	2.758[1]	1.626[-1]	5.839[-2]	3.062[2]
3	9.878[0]	6.780[-1]	5.672[-2]	4.593[2]
4	2.247[1]	1.652[0]	9.325[-2]	4.644[2]
5	3.803[0]	4.468[0]	3.033[-5]	9.946[3]
6	1.840[0]	1.612[1]	2.320[-5]	1.197[8]
7	1.201[0]	4.956[1]	1.193[2]	6.869[9]

increased by about 60% by multi- $n$  CI in both the PP and CP temperature ranges, which leads to the total plasma rate coefficients being increased by up to  $\sim 30\%$  over the PP tem-

perature range. The present FAC and AS  $\Delta N = 0$  plasma rate coefficients agree with experimentally derived values within  $\sim 10\%$  in both the PP and CP temperature ranges. However, the multi- $n$  CI was ignored in the previous calculations [10,14,16], which were lower than the experiment by up to  $\sim 30\%$  over the same temperature ranges.

Additionally, the present DR and TR rate coefficients from 0.2 eV to 0.4 eV are still obviously lower than the experimental values, as shown in Fig. 2. This underestimation will be further investigated.

The present improved quantification of TR rate coefficients for  $\text{Ar}^{14+}$  will be useful for modelers assessing its role in describing non-LTE astrophysical plasma. It is expected that the effect of multi- $n$  CI should also widely exist in other ions, and it needs to be systematically studied. We will present the relevant results and discussion for other ions in our future works.

#### ACKNOWLEDGMENTS

The work of various author(s) was supported by grants from the following programs: National Key R&D Program of China (Contract No. 2022YFA1602500), the UK STFC (Contract No. ST/V000683/1), the National Natural Science Foundation of China (Contracts No. 12074081 and No. U1932207), and the Strategic Priority Research Program of the Chinese Academy of Sciences (Contract No. XDB34020000). We also thank M. F. Gu for providing support in utilizing the FAC potential within AS.

- [1] G. Del Zanna and H. E. Mason, *Living Rev. Sol. Phys.* **15**, 5 (2018).
- [2] K. P. Dere, G. Del Zanna, P. R. Young, E. Landi, and R. S. Sutherland, *Astrophys. J. Suppl. Series* **241**, 22 (2019).
- [3] C. Beilmann, P. H. Mokler, S. Bernitt, C. H. Keitel, J. Ullrich, J. R. Lopez-Urrutia, and Z. Harman, *Phys. Rev. Lett.* **107**, 143201 (2011).
- [4] M. Schnell, G. Gwinner, N. R. Badnell, M. E. Bannister, S. Böhm, J. Colgan, S. Kieslich, S. D. Loch, D. Mitnik, A. Müller *et al.*, *Phys. Rev. Lett.* **91**, 043001 (2003).
- [5] N. R. Badnell, *J. Phys. B: At., Mol. Opt. Phys.* **39**, 4825 (2006).
- [6] I. Orban, S. Böhm, S. D. Loch, and R. Schuch, *Astron. Astrophys.* **489**, 829 (2008).
- [7] I. Orban, S. D. Loch, P. Glans, S. Böhm, and R. Schuch, *Phys. Scr.* **T144**, 014035 (2011).
- [8] S. Schippers, M. Schnell, C. Brandau, S. Kieslich, A. Müller, and A. Wolf, *Astron. Astrophys.* **421**, 1185 (2004).
- [9] I. Orban, S. D. Loch, S. Böhm, and R. Schuch, *Astrophys. J.* **721**, 1603 (2010).
- [10] Z. K. Huang, W. Q. Wen, X. Xu, S. Mahmood, S. X. Wang, H. B. Wang, L. J. Dou, N. Khan, N. R. Badnell, S. P. Preval *et al.*, *Astrophys. J. Suppl. Series* **235**, 2 (2018).
- [11] S. X. Wang, X. Xu, Z. K. Huang, W. Q. Wen, H. B. Wang, N. Khan, S. P. Preval, N. R. Badnell, S. Schippers, and S. Mahmood, *Astrophys. J.* **862**, 134 (2018).
- [12] S. Schippers, E. W. Schmidt, D. Bernhardt, D. Yu, A. Müller, M. Lestinsky, D. A. Orlov, M. Grieser, R. Repnow, and A. Wolf, *J. Phys.: Conf. Ser.* **58**, 137 (2007).
- [13] D. W. Savin, G. Gwinner, M. Grieser, R. Repnow, M. Schnell, D. Schwalm, A. Wolf, S.-G. Zhou, S. Kieslich, A. Müller *et al.*, *Astrophys. J.* **642**, 1275 (2006).
- [14] J. Colgan, M. S. Pindzola, A. D. Whiteford, and N. R. Badnell, *Astron. Astrophys.* **412**, 597 (2003).
- [15] N. R. Badnell, M. G. O'Mullane, H. P. Summers, Z. Altun, M. A. Bautista, J. Colgan, T. W. Gorczyca, D. M. Mitnik, M. S. Pindzola, and O. Zatsarinny, *Astron. Astrophys.* **406**, 1151 (2003).
- [16] M. F. Gu, *Astrophys. J.* **590**, 1131 (2003).
- [17] Available at <http://space.mit.edu/pub/mfgu/fac>.
- [18] Z. K. Huang, W. Q. Wen, S. X. Wang, N. Khan, H. B. Wang, C. Y. Chen, C. Y. Zhang, S. P. Preval, N. R. Badnell, W. L. Ma, X. Liu, D. Y. Chen, X. L. Zhu, D. M. Zhao, L. J. Mao, X. M. Ma, J. Li, M. T. Tang, R. S. Mao, D. Y. Yin *et al.*, *Phys. Rev. A* **102**, 062823 (2020).
- [19] S. Li, J. Q. Li, C. Y. Zhang, K. Wang, K. Yao, Y. Xu, and C. Y. Chen, *J. Quant. Spectrosc. Radiat. Transfer* **232**, 75 (2019).
- [20] M. F. Gu, *Astrophys. J. Suppl. Ser.* **156**, 105 (2005).
- [21] M. F. Gu, T. Holczer, E. Behar, and S. M. Kahn, *Astrophys. J.* **641**, 1227 (2006).
- [22] M. F. Gu, Flexible Atomic Code, v. 1.1.5, 2017 [online], available at <https://www-amdis.iaea.org/FAC/>.

- [23] N. R. Badnell, *Comput. Phys. Commun.* **182**, 1528 (2011).
- [24] V. S. Dubau, J., *Rep. Prog. Phys.* **43**, 199 (1980).
- [25] M. F. Gu, *Can. J. Phys.* **86**, 675 (2008).
- [26] N. R. Badnell, *J. Phys. B: At. Mol. Phys.* **19**, 3827 (1986).
- [27] W. Eissner and H. Nussbaumer, *J. Phys. B: At. Mol. Phys.* **2**, 1028 (1969).
- [28] T. M. Shen, C. Y. Chen, Y. S. Wang, and M. F. Gu, *Chin. Phys. Lett.* **24**, 925 (2007).
- [29] T. M. Shen, C. Y. Chen, Y. S. Wang, Y. M. Zou, and M. F. Gu, *Phys. Rev. A* **76**, 022703 (2007).
- [30] T. M. Shen, C. Y. Chen, Y. S. Wang, Y. M. Zou, and M. F. Gu, *J. Phys. B: At., Mol. Opt. Phys.* **40**, 3075 (2007).
- [31] N. Khan, Z. K. Huang, W. Q. Wen, S. X. Wang, C. Y. Chen, C. Y. Zhang, H. B. Wang, X. Liu, W. L. Ma, D. Y. Chen *et al.*, *J. Phys. B: At., Mol. Opt. Phys.* **55**, 035001 (2022).
- [32] W. Q. Wen, Z. K. Huang, S. X. Wang, N. Khan, H. B. Wang, C. Y. Chen, C. Y. Zhang, S. Preval, N. R. Badnell, W. L. Ma *et al.*, *Astrophys. J.* **905**, 36 (2020).
- [33] W. L. Ma, S. X. Wang, Z. K. Huang, W. Q. Wen, H. B. Wang, D. Y. Chen, X. Liu, X. P. Zhou, H. K. Huang, L. Shao *et al.*, *J. Phys. B: At., Mol. Opt. Phys.* **56**, 095203 (2023).
- [34] X. H. Shi, C. Y. Chen, Y. S. Wang, and M. F. Gu, *Chin. Phys. Lett.* **21**, 1937 (2004).
- [35] F. C. Meng, C. Y. Chen, X. H. Shi, Y. S. Wang, Y. M. Zou and M. F. Gu, *J. Phys. B: At., Mol. Opt. Phys.* **40**, 4269 (2007).
- [36] F. C. Meng, C. Y. Chen, Y. S. Wang, and Y. M. Zou, *J. Quant. Spectrosc. Radiat. Transfer* **109**, 2000 (2008).
- [37] F. C. Meng, L. Zhou, M. Huang, C. Y. Chen, Y. S. Wang, and Y. M. Zou, *J. Phys. B: At., Mol. Opt. Phys.* **42**, 105203 (2009).
- [38] N. R. Badnell, *Astron. Astrophys.* **447**, 389 (2006).
- [39] M. A. Bautista and N. R. Badnell, *Astron. Astrophys.* **466**, 755 (2007).
- [40] J. Colgan, M. S. Pindzola, and N. R. Badnell, *Astron. Astrophys.* **417**, 1183 (2004).
- [41] Z. Altun, A. Yumak, N. R. Badnell, J. Colgan, and M. S. Pindzola, *Astron. Astrophys.* **420**, 775 (2004).
- [42] O. Zatsarinny, T. W. Gorczyca, K. T. Korista, N. R. Badnell, and D. W. Savin, *Astron. Astrophys.* **417**, 1173 (2004).
- [43] D. M. Mitnik and N. R. Badnell, *Astron. Astrophys.* **425**, 1153 (2004).
- [44] O. Zatsarinny, T. W. Gorczyca, J. Fu, K. T. Korista, N. R. Badnell, and D. W. Savin, *Astron. Astrophys.* **412**, 587 (2003).
- [45] O. Zatsarinny, T. W. Gorczyca, J. Fu, K. T. Korista, N. R. Badnell, and D. W. Savin, *Astron. Astrophys.* **447**, 379 (2006).
- [46] O. Zatsarinny, T. W. Gorczyca, K. Korista, N. R. Badnell, and D. W. Savin, *Astron. Astrophys.* **426**, 699 (2004).
- [47] Z. Altun, A. Yumak, N. R. Badnell, S. D. Loch, and M. S. Pindzola, *Astron. Astrophys.* **447**, 1165 (2006).
- [48] Z. Altun, A. Yumak, I. Yavuz, N. R. Badnell, S. D. Loch, and M. S. Pindzola, *Astron. Astrophys.* **474**, 1051 (2007).
- [49] S. A. Abdel-Naby, D. Nikolic, T. W. Gorczyca, K. T. Korista, and N. R. Badnell, *Astron. Astrophys.* **537**, A40 (2012).
- [50] J. Kaur, T. W. Gorczyca, and N. R. Badnell, *Astron. Astrophys.* **610**, A41 (2018).
- [51] E. A. Bleda, Z. Altun, and N. R. Badnell, *Astron. Astrophys.* **668**, A72 (2022).
- [52] N. R. Badnell, *Astrophys. J.* **651**, L73 (2006).
- [53] N. R. Badnell, C. P. Ballance, D. C. Griffin, and M. O'Mullane, *Phys. Rev. A* **85**, 052716 (2012).
- [54] N. R. Badnell, K. Spruck, C. Krantz, O. Novotný, A. Becker, D. Bernhardt, M. Grieser, M. Hahn, R. Repnow, D. W. Savin, A. Wolf, A. Müller, and S. Schippers, *Phys. Rev. A* **93**, 052703 (2016).
- [55] S. P. Preval, N. R. Badnell, and M. G. O'Mullane, *J. Phys. B: At., Mol. Opt. Phys.* **51**, 045004 (2018).
- [56] S. P. Preval, N. R. Badnell, and M. G. O'Mullane, *J. Phys. B: At., Mol. Opt. Phys.* **52**, 025201 (2019).
- [57] D. H. Kwon and D. W. Savin, *Phys. Rev. A* **83**, 012701 (2011).
- [58] A. Peleg, E. Behar, P. Mandelbaum, and J. L. Schwob, *Phys. Rev. A* **57**, 3493 (1998).
- [59] X. L. Guo, R. Si, S. Li, M. Huang, R. Hutton, Y. S. Wang, C. Y. Chen, Y. M. Zou, K. Wang, J. Yan *et al.*, *Phys. Rev. A* **93**, 012513 (2016).
- [60] R. Si, S. Li, X. L. Guo, Z. B. Chen, T. Brage, P. Jönsson, K. Wang, J. Yan, C. Y. Chen, and Y. M. Zou, *Astrophys. J. Suppl. Series* **227**, 16 (2016).
- [61] R. Si, C. Y. Zhang, Z. Y. Cheng, K. Wang, P. Jönsson, K. Yao, M. F. Gu, and C. Y. Chen, *Astrophys. J. Suppl. Series* **239**, 3 (2018).
- [62] C. Y. Zhang, R. Si, Y. W. Liu, K. Yao, K. Wang, X. L. Guo, S. Li, and C. Y. Chen, *At. Data Nucl. Data Tables* **121-122**, 256 (2018).
- [63] C. Y. Zhang, R. Si, K. Yao, M. F. Gu, K. Wang, and C. Y. Chen, *J. Quant. Spectrosc. Radiat. Transfer* **206**, 180 (2018).
- [64] J. Q. Li, C. Y. Zhang, R. Si, K. Wang, and C. Y. Chen, *At. Data Nucl. Data Tables* **126**, 158 (2019).
- [65] Y. T. Li, R. Si, J. Q. Li, C. Y. Zhang, K. Yao, K. Wang, M. F. Gu, and C. Y. Chen, *At. Data Nucl. Data Tables* **133-134**, 101339 (2020).
- [66] K. Wang, D. F. Li, H. T. Liu, X. Y. Han, B. Duan, C. Y. Li, J. G. Li, X. L. Guo, C. Y. Chen, and J. Yan, *Astrophys. J. Suppl. Series* **215**, 26 (2014).
- [67] K. Wang, X. L. Guo, H. T. Liu, D. F. Li, F. Y. Long, X. Y. Han, B. Duan, J. G. Li, M. Huang, Y. S. Wang *et al.*, *Astrophys. J. Suppl. Series* **218**, 16 (2015).
- [68] K. Wang, C. X. Song, P. Jönsson, G. Del Zanna, S. Schiffmann, M. Godefroid, G. Gaigalas, X. H. Zhao, R. Si, C. Y. Chen, and J. Yan, *Astrophys. J. Suppl. Series* **239**, 30 (2018).
- [69] K. Wang, P. Jönsson, G. Gaigalas, L. Radžiūtė, P. Rynkun, G. Del Zanna, and C. Y. Chen, *Astrophys. J. Suppl. Series* **235**, 27 (2018).
- [70] K. Wang, P. Jönsson, G. Del Zanna, M. Godefroid, Z. B. Chen, C. Y. Chen, and J. Yan, *Astrophys. J. Suppl. Series* **246**, 1 (2020).
- [71] C. Y. Zhang, K. Wang, R. Si, M. Godefroid, P. Jönsson, J. Xiao, M. F. Gu, and C. Y. Chen, *J. Quant. Spectrosc. Radiat. Transfer* **269**, 107650 (2021).
- [72] C. Y. Zhang, J. Q. Li, K. Wang, R. Si, M. Godefroid, P. Jönsson, J. Xiao, M. F. Gu, and C. Y. Chen, *Phys. Rev. A* **105**, 022817 (2022).
- [73] E. B. Saloman, *J. Phys. Chem. Ref. Data* **39**, 033101 (2010).

- [74] A. Kramida, Y. Ralchenko, J. Reader, and NIST ASD Team (2020), NIST Atomic Spectra Database (ver. 5.8), [Online]. Available: <https://physics.nist.gov/asd> [2021, January 21]. NIST, Gaithersburg, MD.
- [75] A. V. Malyshev, D. A. Glazov, A. V. Volotka, I. I. Tupitsyn, V. M. Shabaev, G. Plunien, and T. Stöhlker, *Phys. Rev. A* **96**, 022512 (2017).
- [76] See Supplemental Material at <http://link.aps.org/supplemental/10.1103/PhysRevA.108.022801> for Level Table.
- [77] S. Schippers, A. Müller, G. Gwinner, J. Linkemann, A. A. Saghir, and A. Wolf, *Astrophys. J.* **555**, 1027 (2001).
- [78] T. Kallman and M. Bautista, *Astrophys. J. Supp. Ser.* **133**, 221 (2001).
- [79] P. Bryans, E. Landi, and D. W. Savin, *Astrophys. J.* **691**, 1540 (2009).
- [80] Atomic and Molecular Diagnostic Processes in Plasmas, <http://amdpp.phys.strath.ac.uk/index.html>.